IL NUOVO CIMENTO Vol. 25 C, N. 3 Maggio-Giugno 2002

A numerical investigation of the sea breeze and slope flows around Rome(*)

R. Caballero(1) and A. Lavagnini(2)

(1) *Danish Center for Earth System Science, University of Copenhagen - Denmark*
(2) *IFA/CNR - Roma, Italy*

(ricevuto l'1 Febbraio 2001; revisionato il 7 Novembre 2001; approvato il 5 Dicembre 2001)

Summary. — A three-dimensional non-hydrostatic prognostic mesoscale model is used to simulate the circulation around Rome, Italy, on a cloudless summer day with weak synoptic winds, with the aim of characterising the local circulation on such days. The simulation shows that the sea breeze and slope flows play roles of comparable importance. At night the circulation is dominated by katabatic flow. During the late morning/early afternoon there is a sea breeze with a front curving pincer-like around Rome, and well-developed anabatic flows on all slopes. In the late afternoon, sea breeze and slope flows coalesce into a single circulation reaching hundreds of kilometers inland, with an offshore return flow aloft. Comparison with observations is favourable, particularly during the day.

PACS 92.60.Fm – Boundary layer structure and processes.

1. – Introduction

Many of the world's largest and most polluted cities lie in relatively narrow plains hemmed in between the sea and coastal hills or mountain ranges. Given sufficient radiative forcing, these geographic features set up horizontal temperature (and hence pressure) gradients which significantly affect the local atmospheric circulation. Differential heating over land and sea drives the land-sea breeze, which has been very extensively studied [1]. Sloping surfaces generate differential heating by a geometric effect: during the day, air near the surface is heated more than air at the same altitude but farther from the surface, driving low-level anabatic (upslope) flow; at night, the reverse mechanism drives katabatic (downslope) flow. Slope flows have received somewhat less attention, although they can be just as strong as the sea breeze [2]. In a situation where a slope faces the sea, the sea breeze and slope flow move in the same direction and can form a single circulation which is stronger than the separate flows [3].

(*) The authors of this paper have agreed to not receive the proofs for correction.

When thermal forcing is strong and synoptic winds weak, as is often the case in summer, thermally driven flows dominate the local circulation. Because the forcing is geographically fixed and temporally periodic, such flows are particularly tractable. They are of practical importance because they largely determine, among other things, the horizontal and vertical distribution of pollutants. For these reasons, many large coastal cities have had a number of observational and numerical studies dedicated to them, examples being Athens [4, 5], Los Angeles [6, 2, 7] and Tokyo [8, 9].

The city of Rome, which counts 3.5 million inhabitants, lies close to the sea and is surrounded by hills, is another clear candidate, but has to date been less studied. Observational work [10, 11] and [12] has firmly established the importance of the sea breeze in the Rome area, but because the observations were confined to only one or a few points, they could not provide a general, spatially resolved view of the circulation. In particular, there is uncertainty concerning the relative role of slope flows [11]. Numerical simulation, when suitably corroborated by observational data, is the simplest way to obtain such an overview. The main aim of this paper is to present what, to the best of our knowledge, is the first detailed simulation of the summertime circulation around Rome, when not strongly perturbed by synoptic winds.

An important feature of thermally forced flows is that they tend to generate narrow areas of strong convergence and lifting. These occur at the sea-breeze front (SBF), where cool advancing marine air meets warmer land air. They are also observed along ridges, where slope flows on opposite sides of a mountain converge and proceed upwards (the so-called "chimney effect"). These convergence lines are of practical relevance because the high vertical velocities can act to inject pollutants into stable layers above the convective boundary layer (CBL), where they can either remain forming elevated pollution layers [13] or be carried away by the synoptic winds. Further, in a conditionally unstable setting, convergence lines are prime locations for convective initiation [14].

The model we employ is described in the following section. In sect. **3** we give details regarding the set-up for the present simulation. The general features of the simulated circulation are presented in sect. **4**, while the modeled convergence lines are described in sect. **5**. A comparison between simulation results and observations is presented and discussed in sect. **6**. We summarise our results in sect. **7**.

2. – Model description

We employ the mesoscale model MEMO, developed and maintained at the Aristotle University of Thessaloniki, Greece, and at the University of Karlsruhe, Germany. The model has been successfully used in the past to simulate the flow field at various sites (for instance [5,15,16]) and is currently in use by a number of groups and institutions around Europe. We give here only a brief outline of the model to facilitate interpretation of the results presented below; a more detailed description may be found elsewhere [17, 18, 5].

MEMO is a non-hydrostatic prognostic model which solves the continuity and momentum equations and scalar transport equations for temperature, moisture and turbulent kinetic energy on a 3D grid. The vertical coordinate is terrain-following so that complex topography can be included, and the vertical mesh is stretched to give higher resolution in lower layers. Time integration is through an explicit second-order Adams-Bashford scheme (except for the non-hydrostatic and vertical turbulent diffusion terms, which are treated implicitly). Expanded radiation conditions are applied at lateral boundaries, allowing perturbations to travel out of the domain while permitting time-dependent large-scale conditions to be imposed at the boundaries. Sub-grid scale turbulence is modeled

using a one-equation K-closure where the eddy viscosity is diagnosed from the turbulent kinetic energy. Monin-Obukhov similarity theory is applied in the surface layer. The model incorporates a radiative transfer scheme to compute heating rates in the atmosphere and radiative fluxes at the surface. The scheme parameterizes long-wave radiation using the emissivity method, while short-wave radiative transfer is described using an implicit multilayer method; see [19] for details. The model is initialised by interpolating externally supplied wind and temperature data onto the model grid and then correcting the fields to ensure mass conservation. Given the temperature field, moisture is initialised by assuming a constant relative humidity everywhere. The model is "dry" in the sense that no provision is made for moist convection. If air becomes saturated, the excess moisture is simply removed. Naturally, this makes the model suitable only for the simulation of cases (such as the present one) in which it is *known* that moist convection and cloud formation do not occur, or play only a very minor role.

The surface temperature over water is held fixed at a prescribed value, while over land it is determined through the heat balance equation

$$R - Q_{\mathrm{s}} - Q_0 - L_0 = 0,$$

where R is the net radiative flux at the surface, Q_{s} is the heat flux to the sub-surface soil, while Q_0 and L_0 are the sensible and latent heat fluxes to the atmosphere. Q_{s} and sub-surface temperatures are prognostically computed using a multilevel soil model. Q_0 and L_0 are proportional to $T_0 - T_2$ and $q_0 - q_2$, respectively, where T is the temperature, q the specific humidity and subscripts 0 and 2 refer to values at the surface and at the first model level, respectively. The surface Bowen ratio is controlled by specifying an "evaporation parameter" Ψ (with $0 \leq \Psi \leq 1$) and setting

$$q_0 = \Psi q_{\mathrm{s}} + (1 - \Psi) q_2,$$

where q_{s} is the saturation specific humidity at the surface. The value of Ψ depends on the type of surface: moist (dry) surfaces will have high (low) Ψ. The model can accommodate up to seven surface types.

The model also has a nesting facility, so that a simulation may first be run on a large domain using coarse resolution and then re-run with finer resolution on an embedded smaller domain, using output of the coarse run as boundary conditions. This is convenient since thermally forced circulations can extend over hundreds of kilometers but can contain features (such as fronts and convergence lines) with scales on the order of a kilometer or less. Thus it is possible to capture the large-scale behaviour with the coarse-grid simulation and then study small-scale features in the region of interest with the fine-grid run.

3. – Case specification

3˙1. *Domain description.* – The study domain (fig. 1) is roughly centered on the city of Rome, with the coastline running in a fairly straight diagonal line from NW to SE. The city of Rome is situated at the mouth of the Tiber Valley, about 25 km inland from the Tyrrhenian Sea. Near the coast are the large suburbs of Ostia and Acilia. The city is surrounded on three sides by hills: the low Sabatine and Tolfa ranges to the N and NW, the higher Sabine hills to the E and NE and the Alban hills the SE. The Sabine hills are foothills of the Appenines, which rise to considerable height (> 1800 m) towards the NE

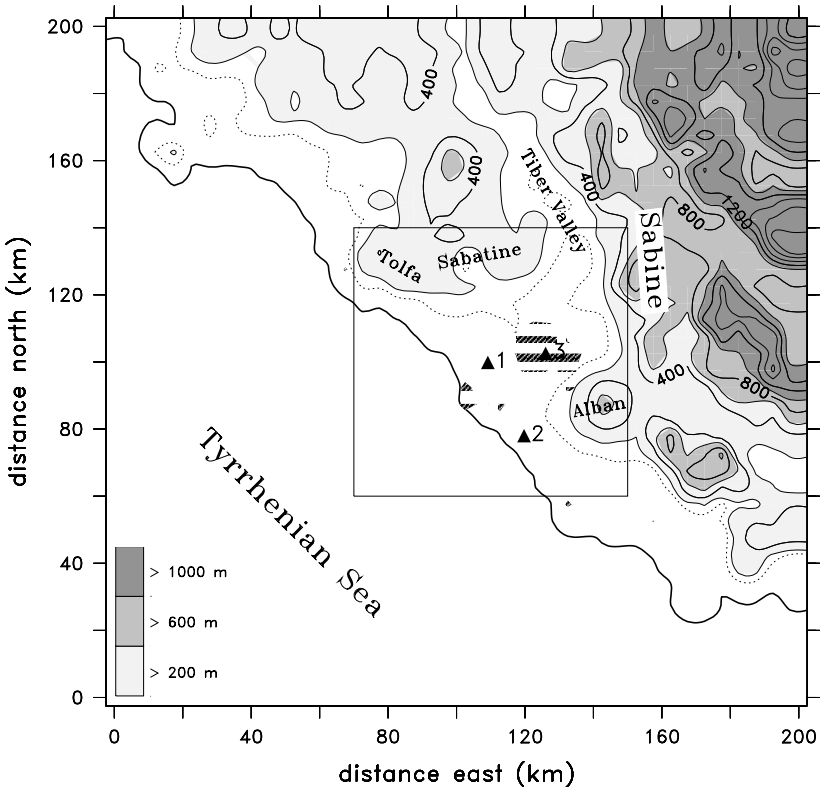

Fig. 1. – The study domain. Full frame shows the 200 × 200 km coarse-grid domain, inset box shows the 80 × 80 km fine-grid domain (see text). Thin contours show topography at 200 m intervals (100 m dotted). Thick contour is the coastline. Hatching shows urban areas. Black triangles indicate the three sodar sites: Ponte Malnome (1), Pratica di Mare (2) and Università di Roma (3).

margin of the domain. We have access to observational data from three sites within the domain (triangles in fig. 1); these data will be compared with model results in sect. **6**.

3˙2. *Model resolution and surface parameters.* – The study is carried out in two nesting stages. We employ a 200 × 200 km coarse-grid domain (full frame of fig. 1) using 5 km resolution, and successively an 80 × 80 km fine-grid domain using 2 km resolution (box in fig. 1). In both runs there are 25 vertical levels reaching a height of 6 km, with 15 levels in the first 1 km above ground level (AGL). The first model level is 10 m AGL. A fine-resolution topographic dataset is available to us; elevations are averaged over each grid box.

The land-use inventory available to us also has fine resolution but contains only four classes. The four classes, with their corresponding evaporation parameter, short-wave albedo and roughness length, are listed in table I. The actual parameter values at each grid box are an average weighted over the percentage of each land-use class contained in the grid box. Areas below 200 m are either urban or farmland; at higher elevations the predominant surface type is forest.

Note that forest areas have similar evaporation parameter to farmland but half the

TABLE I. – *Land-use classes and surface parameters.*

Land-use class	Ψ	albedo	roughness length (m)
Water	1	0	0.001
Farmland	0.15	0.22	0.02
Forest	0.2	0.1	0.12
Urban	0.05	0.2	0.8

albedo and much longer roughness lengths, so surface temperature and sensible heat flux will be higher. Urban areas have similar albedo to farmland but lower Ψ and very much longer roughness length, so again we expect the sensible heat flux to be higher there. Overall, we expect air temperatures to be higher over forests and urban areas than over farmland. The sea surface temperature was fixed at its July climatological value of 23°C.

3˙3. *Synoptic conditions and initialisation*. – The day chosen for simulation is 21 July 1996. Synoptic maps for that day show a small low-level pressure gradient over central Italy inducing weak (about 2 m s^{-1}) offshore gradient wind over the study domain. At 500 hPa there is a trough over Russia and a ridge over North Africa, driving moderate NW winds over most of Italy. Satellite imagery shows cloudless conditions over the study domain.

The model was initialised using a single radiosounding taken at Pratica di Mare (see fig. 1) on 21 July at 0100 Local Standard Time (LST, corresponding to Central European Time, an hour ahead of UTC and about half an hour behind local solar time). The sounding exhibits a weak inversion at around 2 km (most probably a residue of the daytime CBL top) and a mean free-atmosphere lapse rate of 7 K km^{-1}. Mean relative humidity below 2 km is around 70%. Wind speeds and directions are consistent with those observed in the synoptic maps mentioned above. The run was started at 1800 LST of the previous day, the first 6 hours being treated as a spin-up phase. The real simulation started at 0000 LST of 21 July.

4. – Diurnal evolution of the simulated circulation

In this section we describe the general features of the simulated circulation by studying the fine-grid results at four representative time slices: 0500 LST (mature nocturnal regime), 1100 LST (morning transition), 1700 LST (mature daytime regime) and 2100 LST (evening transition). Sunrise and sunset are at 0450 and 1940 LST, respectively.

4˙1. *Nocturnal regime*. – The nocturnal regime (fig. 2a) appears dominated on land by katabatic slope flows down the major topographic features, with surface winds roughly perpendicular to elevation contours everywhere. North of Rome, flow down the Sabatine and Sabine ranges converges at the valley floor and is funneled toward the city. Air flowing down the northern slopes of the Alban hills also meets air from the Sabine range and is turned west, so that a fairly uniform NE flow reaches the city. The flow is significantly slowed over the city due to the high roughness there. There is also some backing over the city, perhaps because of mixing with the NW flow at higher levels.

The vertical structure (fig. 3a) exhibits a very stable boundary layer over land with a depth of some 200 m where the seaward flow is concentrated. The stable layer is advected offshore forming a front at around 20 km from the coast, where there is significant upward

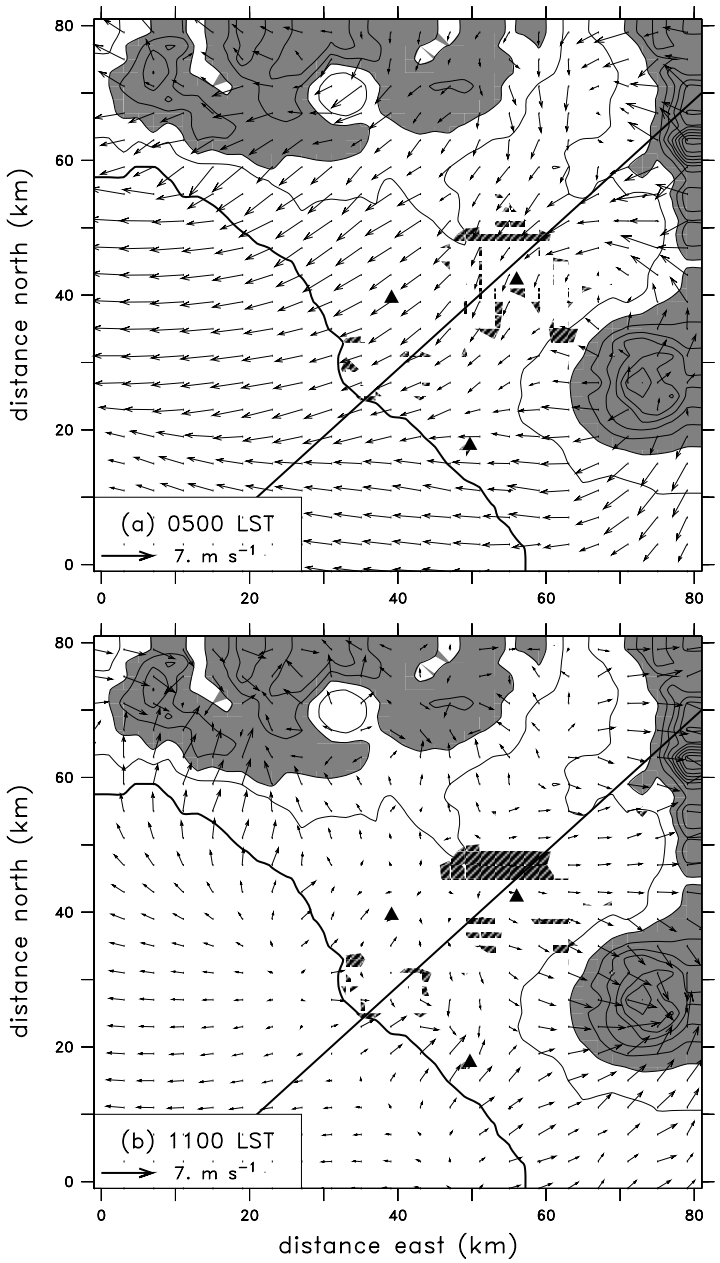

Fig. 2. – Horizontal wind in the first model level (10 m AGL) at (a) 0500 LST and (b) 1100 LST. Contouring shows topography at 100 m intervals. Shading shows elevations > 200 m. Black triangles show the sodar sites (see fig. 1). Hatching shows urban areas. Thick diagonal lines indicate the position of the vertical sections shown in fig. 3.

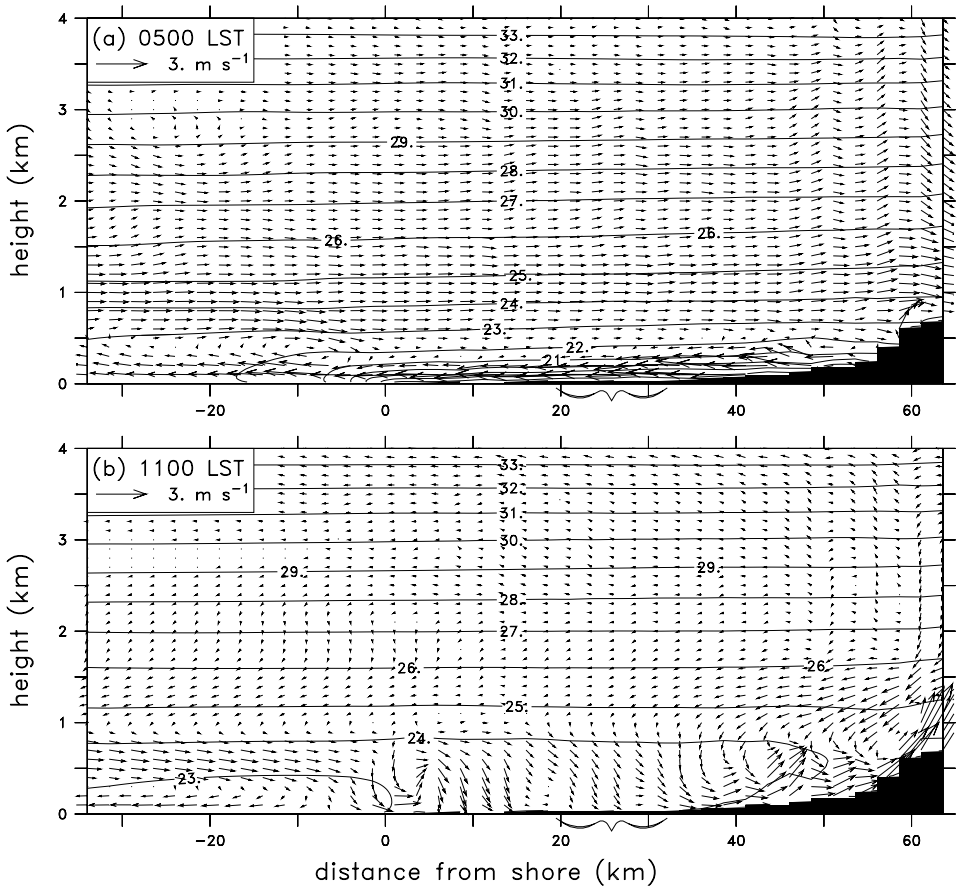

Fig. 3. – Vertical sections through the domain at (a) 0500 LST and (b) 1100 LST (the position of the sections is shown in fig. 2). Arrows show wind projected onto the plane of the section (for display purposes, vertical component is multiplied by a factor of 10). Contours show potential temperature at intervals of 1°C. The bracket below each panel shows the position of the city.

air motion. There is a rather weak return flow centered at an altitude of 1 km. The return flow downwells in the region behind the front, but a weak branch continues on inland reaching the hills in the north of the domain. Overall, we may characterise the nocturnal regime as a single katabatic-land breeze circulation encompassing the whole domain with a total depth of about 1 km.

4˙2. *Morning transition.* – By 1100 LST, the circulation on land (fig. 2b) is almost exactly the reverse of that observed at night. The wooded slopes heat up quickly after sunrise and strong anabatic circulations are set up; surface winds are again perpendicular to elevation contours, but pointing uphill. The fairly straight Sabine range to the NE of Rome induces an almost parallel flow which reaches down into the Tiber valley and affects the eastern part of the city. South and SE of the city, the air is flowing towards the Alban hills, while to the north it flows towards the Sabatine range. At the coast, a sea breeze is firmly established to the NW and SE of Rome, but is only incipient in

the center of the domain around Ostia. Clearly, the presence of the Tolfa range and the Alban hills near the shore favours quick inland penetration of the sea breeze there, while the high roughness of Ostia-Acilia perhaps has a retarding effect. This lends a curved shape to the SBF which is probably a characteristic feature on days (such as this one) not strongly affected by synoptic winds. In the area between the coast and the city, and over the city itself, winds are very weak and disorganised.

The vertical section (fig. 3b) shows that the CBL over low-lying areas has reached a depth of some 800 m. The marine boundary layer is about 400 m deep. The incipient sea breeze circulation is clearly visible as a (horizontal-axis) vortex at the shoreline; so is the much stronger circulation associated with the anabatic slope flow, which extends over some 30 km.

4˙3. *Daytime regime.* – During the afternoon the SBF progresses across the domain, maintaining its curved shape, until at around 1700 LST (fig. 4a) it reaches the Sabine range, whereupon a separate sea breeze system cannot be distinguished from the slope flow. At this point the flow is fairly uniform and directed more or less perpendicularly inland from the coast. The strong flow and weak vertical stratification mean there is little orographic modification of the streamlines. The vertical section (fig. 5a) shows that the flow system reaches considerable depth: the onshore flow is around 1 km deep, while the return flow is about twice as deep. Note that the return flow is roughly centered around CBL top, which approaches 3 km AGL. Note also that the synoptic wind is directed orthogonally to the plane of the section, so the flow aloft in the figure must be attributed to the thermally forced circulation. The flow appears as a single circulation covering the whole domain; indeed, examination of a similar section for the coarse-grid domain shows a single circulation stretching more than 260 km and completely filling the grid. The great depth achieved by the flow system is in part be due to the weak background stratification, which allows the CBL to become very deep. Lu and Turco [13], in a numerical study with a configuration somewhat similar to ours (a 1.5 km mountain near an ocean) but with a strong capping inversion at 1 km height, found the return flow centered at the height of the inversion.

4˙4. *Evening transition.* – After sunset, the land surface quickly cools off and the temperature gradients driving the circulations disappear, but by inertia the circulation retains its daytime structure for some time, as is evident in figs. 4b and 5b. However, air parcels moving onshore at low levels now encounter a stable stratification when moving uphill, so they are forced to move around rather than over obstacles. This leads to quite conspicuous channeling of the flow into the Tiber Valley north of the city.

5. – Convergence lines and updrafts in the daytime CBL

We give here some more detail regarding the structure and time evolution of the convergence lines set up by the thermally forced circulation. We select two time-slices, corresponding to the moment when the SBF passes over the sodar station at Ponte Malnome (1230 LST) and over downtown Rome (1430 LST).

The situation at 1230 LST (fig. 6a) is rather complex, but the SBF can be recognised as a somewhat ragged line of strong upwelling running from Lake Bracciano (the circular feature NW of Rome, between the Tolfa and Sabatine ranges) to the Alban hills tracing a broad curve. Frontal convergence and lifting are particularly strong near the Alban hills, where the cooler marine air collides at right angles with the warm upslope circulation.

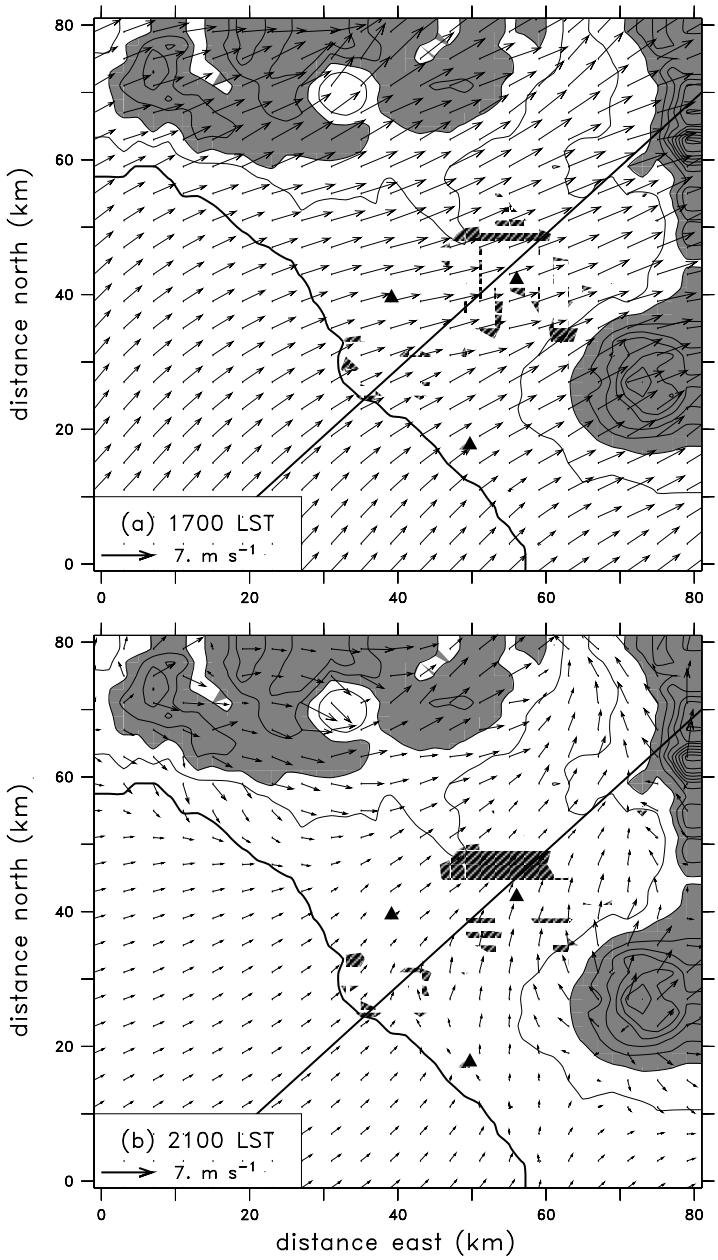

Fig. 4. – As in fig. 2 but at (a) 1700 LST and (b) 2100 LST.

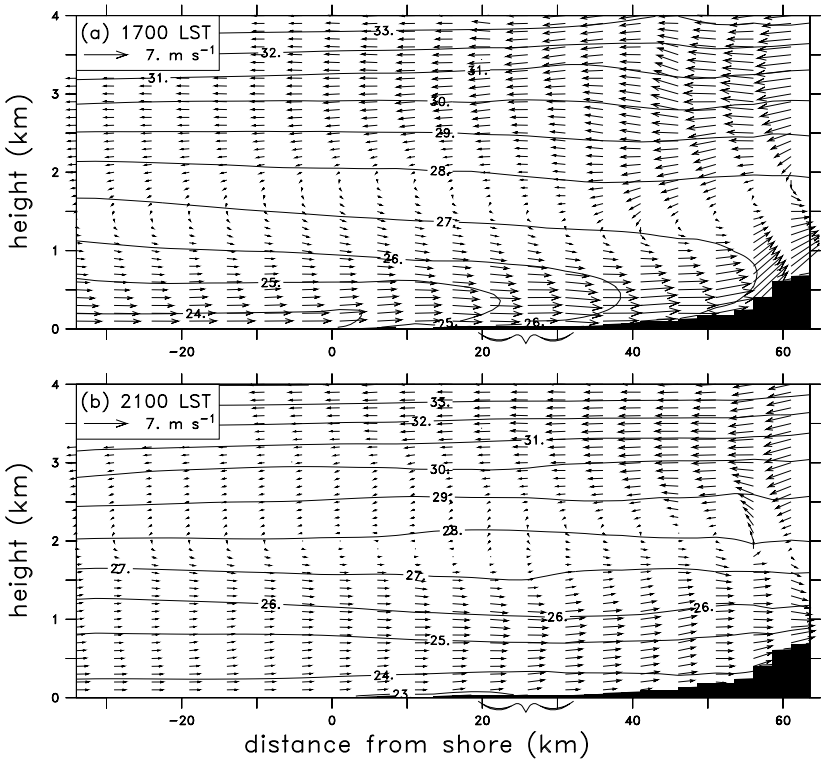

Fig. 5. – As in fig. 3 but at (a) 1700 LST and (b) 2100 LST.

Convergence lines with associated strong updrafts can also be seen around the rim of Lake Bracciano and along the ridge of the Sabatine range. These arise through the "chimney effect" described in the Introduction.

Inland of the SBF, to the W and N of the city, the vertical velocity field features patchy areas of up- and downwelling with scales of only a few kilometers, sometimes forming striated patterns. These look rather like convective cells and rolls [20,21]. These features would be of some interest if truly present in the circulation; unfortunately, they are too poorly resolved in the present simulation to warrant further study.

By 1430 LST, the situation has evolved considerably (fig. 6b). The SBF, which is now passing over downtown Rome, still has its curved shape but is stronger and better defined. It is informative to examine a section normal to the SBF at this time (fig. 7). Seaward of the SBF at low levels, we see the typical wedge-shaped structure of the sea breeze circulation's onshore branch (see, for instance, [22]), which has a maximum speed of about 5.5 m s^{-1} at 200 m AGL and a very well-defined front. Vertical temperature advection at the front is strong enough to locally lift CBL top by about 300 m. Behind the front, the CBL is much shallower because of horizontal advection of cooler marine air. Aloft behind the front, there is a region of weak downwelling and a return flow with speeds of 1–2 m s^{-1}.

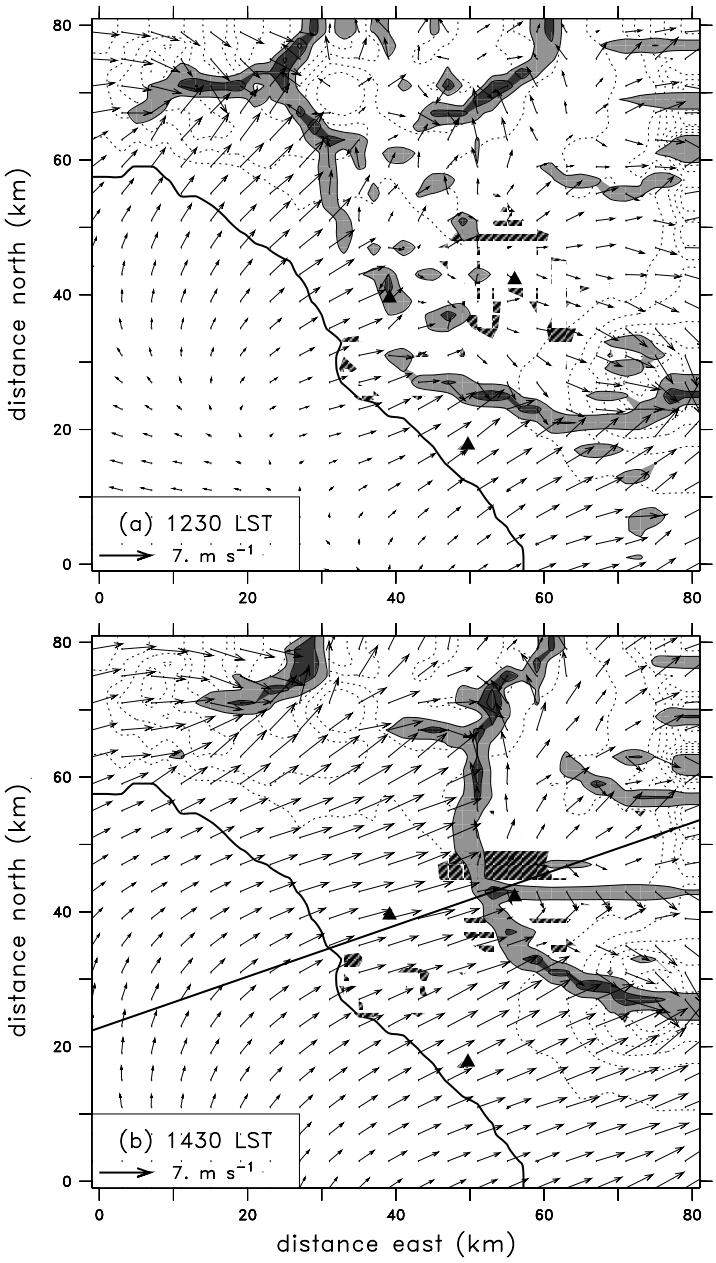

Fig. 6. – Horizontal and vertical winds at (a) 1230 LST and (b) 1430 LST. Arrows show horizontal wind in the first model level (10 m AGL). Light (dark) shading shows upwelling at 400 m AGL with speed > 0.2 m s^{-1} (> 0.8 m s^{-1}) at the same level. Diagonal hatching shows urban areas. Dotted contours show topography at 100 m intervals. Black triangles show the sodar sites (see fig. 1). The thick diagonal line indicates the position of the vertical section shown in fig. 7.

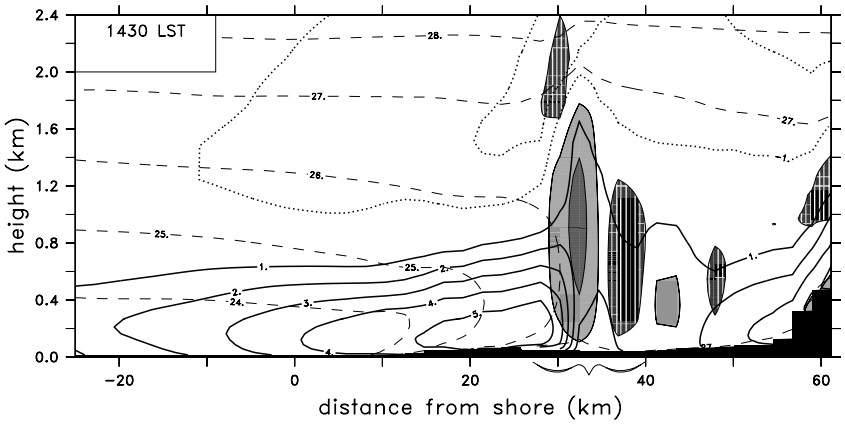

Fig. 7. – Vertical section across the SBF at 1430 LST, when it is passing over the city of Rome. The section's position is shown by the thick diagonal line in fig. 6b. Thick contours show horizontal wind component parallel to the section (positive onshore). Contour interval is 1 m s^{-1}, negative contours dotted, zero contour omitted. Light (dark) shading shows upwelling with speed > 0.2 m s^{-1} (> 1 m s^{-1}). Vertical hatching shows downwelling with speed in excess of 0.2 m s^{-1}. Thin dashed contours show potential temperature at 1°C intervals. The bracket under the figure shows the position and extent of the city.

6. – Comparison with observations

To corroborate the simulation results, we compare them here to observations taken on the simulated day. Two sets of observational data are available to us:

i) Doppler sodar data from three sites (fig. 1):

Site 1: Ponte Malnome, in open farmland 10 km from the coast, at an altitude of 65 m above sea level (ASL);

Site 2: Pratica di Mare, near the coastline south of the city, altitude 20 m ASL;

Site 3: Università di Roma, in downtown Rome, altitude 60 m ASL.

Data from sites 1 and 3 has been analysed in [11], which also gives technical details on the instrumentation. The data are provided as half-hour means and variances of horizontal and vertical velocities at ranges between 40 and up to 900 m AGL; however, due to missing data, a meaningful comparison cannot be made above 400 m (200 m in the case of site 3).

ii) Radiosoundings from Pratica di Mare (site 2 above). These are conventional soundings routinely carried out by the Air Force Meteorological Service daily at 0100, 0700, 1300 and 1900 LST.

6˙1. *Low-level winds*. – Here we compare time-series of model and sodar-derived horizontal and vertical velocities at the three sites. Model values correspond to the grid point closest to the sodar station and are vertically interpolated to the level of the measurements.

In fig. 8 we compare horizontal wind speeds and directions at 70 m AGL. At all sites, horizontal wind speeds exhibit two maxima, one around dawn (nocturnal regime,

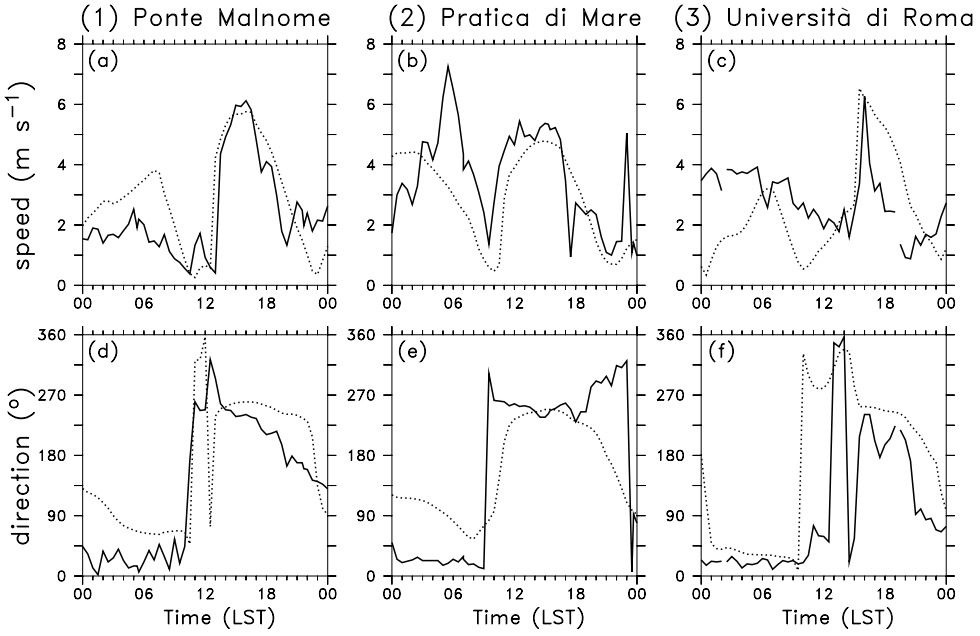

Fig. 8. – Comparison of observed (solid line) and simulated (dotted) horizontal wind speed (a-c) and direction (d-f) 70 m AGL over the three sodar sites (fig. 1). Gaps in solid lines indicate missing data.

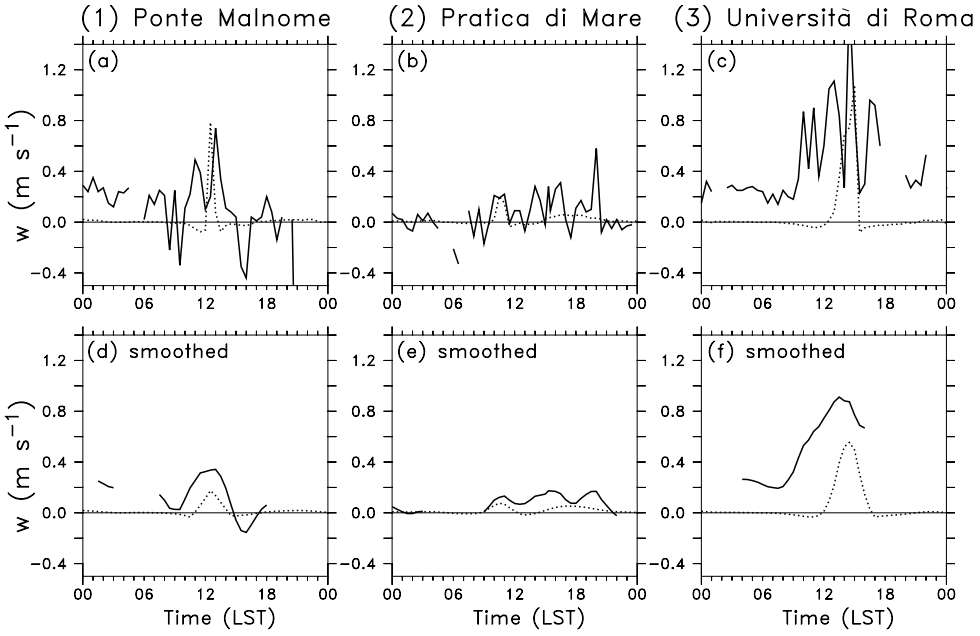

Fig. 9. – Comparison of observed (solid line) and simulated (dotted) vertical velocity 400 m AGL over the three sodar sites (fig. 1). Panels (a)-(c) show the half-hourly values; panels (d)-(f) show the data but smoothed with a 7-point Parzen (triangular) filter. Gaps in solid lines indicate missing data.

subsect. **4**˙1) and one in the afternoon (daytime regime, subsect. **4**˙3). A three-month summer average of the observations (computed in [12] for Ponte Malnome) shows the same structure with similar peak values, indicating that our simulation day is indeed a "typical" day. Although the sodar data have considerably more variability than the model data, it is clear that the daytime evolution is reasonably well captured (particularly at Ponte Malnome), with the maxima occurring at the right times and with the correct values. The nocturnal regime, on the other hand, is less well simulated.

Wind direction is also predicted better during the day than at night. Site 3 (fig. 8f) is an exception, showing that the NE wind direction over Rome at night, due to the Tiber Valley drainage flow (subsect. **4**˙1) is found also in the sodar data. The direction switches to westerly at around 1000 LST in the model, due to the Sabine range's slope flow (subsect. **4**˙2), but this appears to happen 3 hours later in the sodar data. At Pratica di Mare (fig. 8e), wind direction is badly predicted after 1800 LST. We account for this as follows. As the land cools down after sunset, the wind is forced to flow around hills rather than over them (subsect. **4**˙4). Thus, upwind of a hill, there is a region of diffluence where the flow divides into branches turning right and left around the hill. Pratica di Mare is close to the diffluence associated with the Alban hills (see fig. 4b). It appears that the model places this diffluence too far south; the reason for this is not entirely clear, but is probably connected with mixing with the flow aloft, which, as we will see below, is incorrectly predicted to back instead of veer with height in the evening. Note also that wind direction can exhibit high variability even in the model (see in particular fig. 8d), with changes of more than 90° in 30 minutes; we return to this point below.

The difference between the model's daytime and nighttime skill may be due to a number of causes. Firstly, the nocturnal circulation is dominated by katabatic flow (subsect. **4**˙1) which is difficult to predict since it is very shallow and sensitive to details of the topography that may be smoothed out on the grid. It is well known also that turbulence closure schemes tend to perform poorly in stable boundary layers. Further, some experimentation has also shown that the nocturnal regime is sensitive to initialisation, which does not affect the more vigorous daytime flow. Uncertainties in humidity (which affects surface cooling rates through its effect on both evaporation and infrared radiation) will also play a role. In any case, the match with observations is good enough to at least qualitatively corroborate the characterisation of the nocturnal flow given in subsect. **4**˙1.

In fig. 9 we compare vertical velocities at 400 m AGL. We again note (fig. 9a-c) the much higher variability in sodar data than in model output. At all 3 sites, modeled vertical velocities exhibit a single, intense positive spike in the late morning/early afternoon (though at Pratica di Mare there is also a broader peak later in the afternoon). The spikes correspond very well, in both intensity and timing, with similar spikes in the sodar data (apart from some underestimation at Università di Roma, fig. 9c). The spikes coincide with an abrupt increase in horizontal wind speed accompanied by a roughly 180° shift in direction (fig. 8), and correspond to the passage overhead of the SBF (see fig. 6a,b). We conclude therefore that the model is accurately simulating the inland penetration of the sea breeze and the convergence at the SBF.

However, the sodar data in fig. 9a-c shows a number of other positive and negative spikes which are not present in the model. We conjecture that they are due to sub-grid-scale convective structures (note in fact that the variability is much stronger during the day than at night). When such structures are advected over an observation point by the ambient wind, the passage of an updraft (downdraft) will produce a positive (negative) spike. This fine-scale vertical velocity field is superposed on larger-scale fields, such as that generated by the SBF. Indeed, if we average over the high-frequency fluctuations by

applying a running-mean filter to the time series (fig. 9d-f), we see that only the peaks connected with the SBF remain (though broadened by the smoothing). Furthermore, mass continuity implies that local up- or downdrafts will affect near-surface horizontal wind speed and direction, and could account for much of the high-frequency variability observed in fig. 8. In fact, an example of this behaviour may be found in the model itself. At 1230 LST, the SBF is over Ponte Malnome (fig. 6a) and is strongly modulated there, apparently through interaction with a convective cell; this coincides with some very rapid fluctuations in horizontal wind direction, as shown in fig. 8d.

Finally, we note that the vertical velocities in the sodar records (fig. 9) tend to show positive time-mean values. In particular, the records at Ponte Malnome and Università di Roma exhibit a fairly constant value of about 0.2 m s^{-1} through the night. This suggests there may be a problem with instrument calibration, leading to positive systematic error in the velocity readings. Even if this is so, we expect the bias to be constant in time and hence have little or no influence on the time variability of the signal.

6˙2. *Vertical profiles*. – We now compare data from the soundings at Pratica di Mare with vertical profiles from the nearest model point. We note first that a comparison between radiosounding and sodar winds (not shown) reveals reasonable agreement in direction, but differences of 2 m s^{-1} or more in speed. Radiosounding wind speeds, measured by balloon tracking, are known to be inaccurate. Thus, we feel that a comparison of radiosounding and model wind speeds (which also shows differences of around 2 m s^{-1}, not shown) is not meaningful, and we will focus on potential temperature and wind direction.

At 0700 LST (fig. 10a,b), the sounding shows an extremely stable low-level temperature structure, reflecting a cool land breeze overlaid by a warmer return flow. Indeed, wind direction indicates offshore flow near the surface, backing to onshore flow centered around the 500 m level. In the model, the vertical temperature gradient is weaker, perhaps indicating excessive vertical mixing, and the flow veers with height. In both cases, agreement is excellent above 500 m.

At 1300 LST, the top of the CBL can with some difficulty be detected in the model data as a kink in the temperature profile at around 2 km (fig. 10c), while it is more visible in the sounding. There is evidence of an internal boundary layer between the surface and 800 m, coinciding with the onshore branch of the sea breeze (bear in mind that Pratica di Mare is very close to the coast). Wind directions (fig. 10d) indeed show onshore flow up to 800 m and offshore flow aloft up to the CBL top, with the synoptic NW flow above. This structure is very well captured by the model.

The sounding at 1900 LST shows a similar temperature structure (fig. 10e), but with CBL top now at about 3 km AGL and with a well-defined 1 km-deep internal boundary layer. The model matches the observed temperature well at the surface, but gives a 1 K overestimate in the internal boundary layer and a smaller one up to CBL top. Wind direction in the sounding (fig. 10f) is onshore up to 1 km and offshore above up to CBL top, again with NW flow further aloft. The model faithfully reproduces the onshore branch, but departs significantly from observations aloft. We believe this discrepancy is due to the fact that the coupled sea breeze-slope flow circulation has by now reached dimensions exceeding that of the (coarse-grid) domain, leading to a distorted representation of the return flow. We note, however, that the offshore flow aloft seen in the sounding (fig. 10f) implies that a return flow *is* present (c.f. [23], where no return flow is detected in observations of the sea breeze in Monterey).

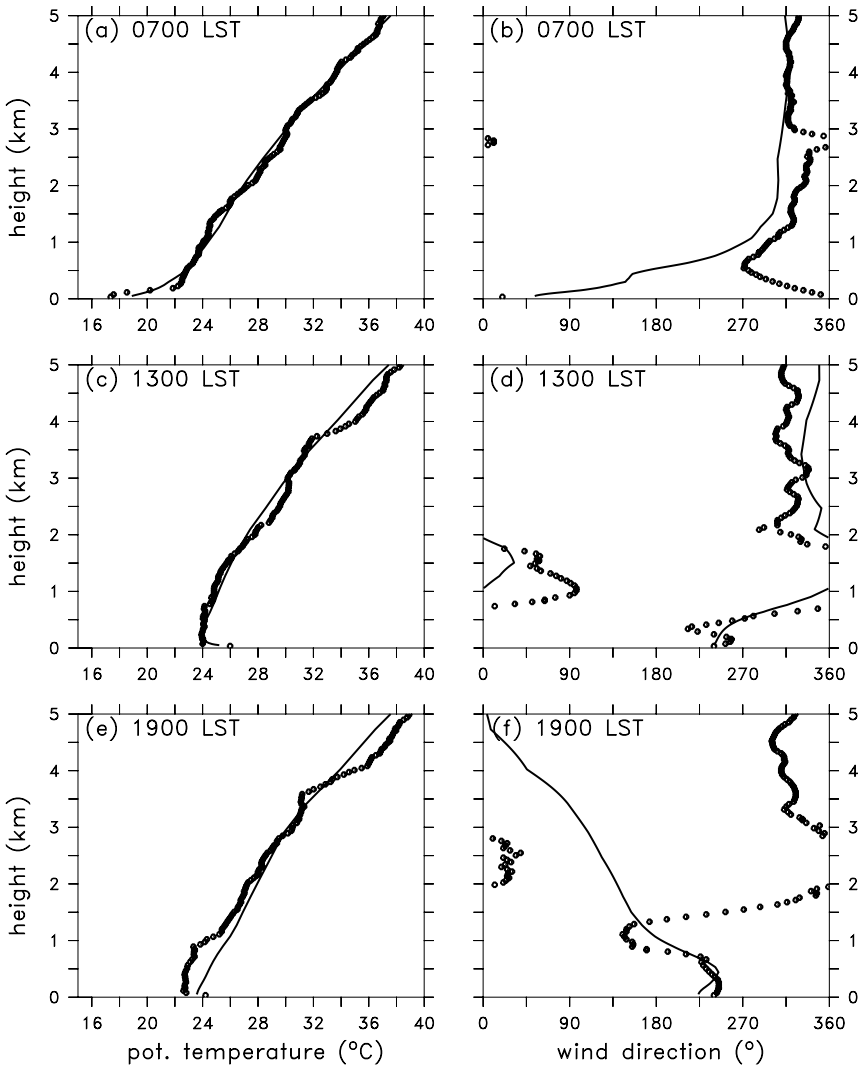

Fig. 10. – Comparison of radiosounding-observed (circles) and simulated (solid line) potential temperatures and wind direction over Pratica di Mare at 0700 LST (a,b), 1300 LST (c,d) and 1900 LST (e,f).

7. – Conclusions

Using a non-hydrostatic prognostic mesoscale model, we have simulated the circulation around Rome on a cloudless summer day with weak synoptic winds, with the aim of characterising the local circulation on such days and studying some of its finer-scale features.

Concerning the characterisation of the flow, our main conclusion is that sea breeze and slope flow effects play roles of comparable importance. A similar conclusion was reached by Ulrickson and Mass [2] in their study of the circulation in the Los Angeles basin. We summarise the main features of the circulation around Rome as follows. At night, the

circulation is dominated on land by katabatic flow, which converges on the plains NE of Rome and travels south-westward over the city on its way to the sea. This seaward flow is around 100 m deep and very stable, and there is a return branch aloft. In the morning, anabatic flow on the Tolfa and Alban hills promotes rapid inland penetration of the sea breeze to the S and NW of the city, while penetration is slower around Ostia-Acilia, lending a curved shape to the SBF. The SBF detaches itself completely from the coastline between 1100 and 1200 LST, progressing inland at an average speed of about 10 km h^{-1} while maintaining its curved shape. Through the afternoon, vertical velocities in the SBF are typically in excess of 1 m s^{-1}. The SBF passes over Rome between 1400 and 1500 LST and reaches the Sabine hills at around 1700 LST. After this time, separate sea breeze and slope flow circulations cannot be distinguished; there is a single circulation reaching hundreds of kilometers inland. The onshore branch of this circulation has a depth of 1 km, a typical near-surface speed of 6 m s^{-1}, and an offshore return flow aloft.

A limitation of the present study is the use of a domain size (200 km) comparable to the size of the mature sea breeze/slope flow circulation. This will probably constrain the structure of the flow, in particular of the upper branch or return flow, and make the simulation sensitive to the boundary conditions. A larger domain size should be used in future studies. It would also be worthwhile to carry the nesting a step further and conduct very fine-scale simulations (grid spacing of 500 m or less) to determine whether convective cells or rolls can indeed form and, if so, study how they interact with the SBF.

* * *

We thank Prof. N. MOUSSIOPOULOS and collaborators at the Laboratory for Heat Transfer and Environmental Engineering, Aristotle University of Thessaloniki, Greece, for providing us with the MEMO model and for the help and hospitality offered to one of us (RCA) as a visitor to the laboratory. We are also grateful to Drs. P. MASTRANTONIO, S. ARGENTINI and A. VIOLA for providing us with the sodar and radiosonde data, and to C. TRANSERICI for computational support at IFA/CNR. Work partially financed by Agenzia Spaziale Italiana and Italy-Greece bilateral Project No. 5672/30.5.97, and by Dansk Grundforskningsfond.

REFERENCES

[1] SIMPSON J. E., *Sea Breeze* and *Local Circulation* (CUP, Cambridge) 1994.
[2] ULRICKSON B. L. and MASS C. F., *Mon. Weather Rev.*, **118** (1990) 2162.
[3] MARHER Y. and PIELKE R. A., *Mon. Weather Rev.*, **105** (1977) 1151.
[4] PREZERAKOS G. P., *Boundary-Layer Meteorol.*, **36** (1986) 245.
[5] KUNZ R. and MOUSSIOPOULOS N., *Atmos. Environ.*, **29** (1995) 3575.
[6] GLENDENING J. W., ULRICKSON B. L. and BUSINGER J. A., *Mon. Weather Rev.*, **114** (1986) 2537.
[7] LU R. and TURCO R. P., *Atmos. Environ.*, **29** (1995) 1499.
[8] KURITA H., UEDA H. and MITSUMOTO S., *J. Appl. Meteorol.*, **29** (1990) 131.
[9] YOSHIKADO H., *J. Appl. Meteorol.*, **31** (1992) 1146.
[10] COLACINO M., and DELL'OSSO L., *Boundary-Layer Meteorol.*, **14** (1978) 133.
[11] MASTRANTONIO G., VIOLA A. P., ARGENTINI S., FIOCCO G., GIANNINI L., ROSSINI L., ABBATE G., OCONE R. and CASONATO M., *Boundary-Layer Meteorol.*, **71** (1994) 67.
[12] LEUZZI G. and MONTI P., *Nuovo Cimento C*, **20** (1997) 343.
[13] LU R. and TURCO R. P., *J. Atmos. Sci.*, **51** (1994) 2285.
[14] NICHOLLS M. E., PIELKE R. A. and COTTON W. R., *Mon. Weather Rev.*, **119** (1991) 298.

[15] Moussiopoulos N., Sahm P., Kunz R., Vögele T., Schneider Ch. and Kessler Ch., *Atmos. Environ.*, **31** (1997) 3177.
[16] Schneider Ch., Kessler Ch. and Moussiopoulos N., *Atmos. Environ.*, **31** (1997) 3187.
[17] Moussiopoulos N., *Fortschr.-Ber. VDI*, **15** (1989).
[18] Flassak Th., *Fortschr.-Ber. VDI*, **15** (1990).
[19] Moussiopoulos N., *Envir. Software*, **2** (1987) 172.
[20] LeMone M. A., *J. Atmos. Sci.*, **30** (1973) 1077.
[21] Weckwerth T. M., Wilson J. W., Wakimoto R. M. and Crook N. A., *Mon. Weather Rev.*, **125** (1997) 505.
[22] Finkele K., Hacker J. M., Kraus H. and Byron-Scott R. A. D., *Boundary-Layer Meteor.*, **73** (1995) 299.
[23] Banta R. M., Olivier L. D. and Levinson D. H., *J. Atmos. Sci.*, **50** (1993) 3959.